Birefringence and Depolarized Light Scattering from Ordered Block Copolymers with Anisotropic Distributions of Grain Orientations Produced by Shear Flow

Ferass M. Abuzaina,† Bruce A. Garetz,*,† Jatin U. Mody,† Maurice C. Newstein,† and Nitash P. Balsara*,‡

Department of Chemical & Biological Sciences & Engineering and Department of Electrical Engineering, Polytechnic University, Brooklyn, New York 11201, and Department of Chemical Engineering and the Materials Sciences Division and Environmental Energies and Technologies Division of Lawrence Berkeley National Laboratory, University of California, Berkeley, California 94720

Received December 1, 2003; Revised Manuscript Received February 20, 2004

ABSTRACT: We have observed birefringence and depolarized light scattering patterns with 2-fold symmetry from a cylindrical diblock copolymer solution that was ordered under shear flow. We have developed a theory to account for such 2-fold symmetric scattering patterns, based on a model that assumes an anisotropic orientation distribution of ellipsoidal grains in the sample. We also show how scattering patterns can be approximately reduced to the sum of three terms of the form $C_n(\theta)\cos(n\phi)$, where θ and ϕ are polar angles in the detection plane and $n = 0$, 2, and 4. By comparing the experimentally determined $C_n(\theta)$ functions with theoretical calculations, we estimated the fraction of the sample that is composed of misaligned grains, their size and eccentricity, and the angular range over which their optic axes were distributed ($\Delta\Theta$). The analysis of the optical properties of these kinds of systems is complicated by the fact that the signal from misaligned grains diminishes extremely rapidly as $\Delta\Theta$ decreases.

Introduction

Considerable theoretical and experimental effort has led to the identification of the factors that govern the symmetry and size of ordered domains that form spontaneously in block copolymer melts.[1−8] There is an increasing interest in using block copolymer domains in applications such as lithographic templates and high-density information storage.[9,10] Chaikin, Register, and co-workers demonstrated that block copolymer templates could be used to make 20 nm holes in a silicon nitride substrate.[9] Russell and co-workers have grown cobalt nanowires from a gold surface using a block copolymer scaffold.[10] The uniformity and density of nanostructures (about 10^{11}/cm^2) achieved in these studies is impressive. However, in addition to high density, applications in the areas of lithography and information storage require stringent control over long-range order or, equivalently, exceptionally low defect density. Current understanding of the factors that govern long-range order in block copolymers is extremely limited.

Observations in position space using techniques such as transmission electron microscopy (TEM) and atomic force microscopy (AFM) provide one avenue for studying the extent of long-range order in block copolymers.[11−14] AFM has been particularly effective for studying defect structure and dynamics in two-dimensional systems.[15−21] In principle, similar studies could be conducted in three-dimensional samples using transmission electron microtomography (TEMT).[22−24] However TEMT studies are currently restricted to determination of local domain structure in block copolymers and related systems.

Over the past decade, our group has used depolarized light scattering (DPLS) to study long-range order in block copolymers.[25−27] This technique can only be used to study anisotropic structures such as lamellae and cylinders arranged on a hexagonal lattice. Ordered single crystals composed of either lamellae or cylinders are uniaxially birefringent with optic axes perpendicular to the lamellae or parallel to the cylinder axes. The extremely weak birefringence of these materials ($\Delta n \sim 10^{-4}$) gives rise to very weak scattering such that the Born approximation is valid and multiple scattering can be neglected.[25] In addition, typical ordered domain (grain) sizes are on the order of 1−10 μm, sufficiently larger than the wavelength of the of the incident light that the paraxial approximation is also valid.[25] The earliest studies considered samples composed of randomly oriented "ideal" grains: uncorrelated grains whose optic axes are uncorrelated with their shapes.[25] More complex systems have included samples containing ellipsoidal grains whose optic axes lie along their shape axes,[26] and samples consisting of correlated clusters of ellipsoidal grains.[27] Recently, theoretical justification for the assumption of ellipsoidal grains has been derived.[28,29]

The application of external fields such as shear flow and electric fields leads to alignment of block copolymer domains.[30−48] If the alignment were perfect, then the entire macroscopic sample would be a uniaxial single crystal. While extremely good alignment is sometimes reported in the literature, there is no evidence that entirely defect-free samples can be produced. Aligned samples are thus composed of two kinds of ordered regions: a macroscopic single crystal that coexists with a set of misaligned grains. In a previous study,[30] it was demonstrated that a combination of birefringence and depolarized light scattering could be used to characterize such systems. The birefringence measurements enabled characterization of the single crystal, while depolarized light scattering measurements enabled characterization of the misaligned grains. If the optic axes of the misaligned grains are randomly oriented, then the resulting depolarized light scattering will

* To whom correspondence should be addressed.
† Polytechnic Unviersity.
‡ Unversity of California, Berkeley.

10.1021/ma035808t CCC: $27.50
Published on Web 04/28/2004

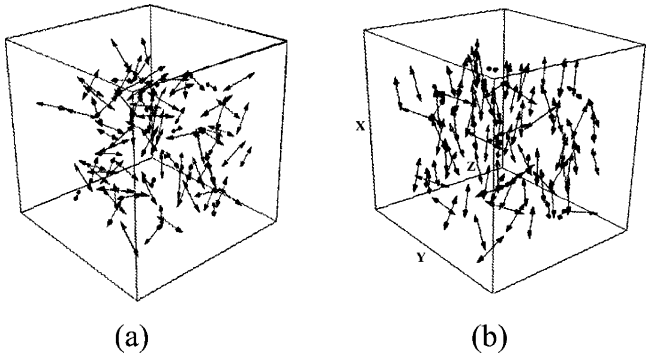

Figure 1. Schematic representation of (a) an isotropic orientation distribution and (b) an anisotropic orientation distribution of ellipsoidal grains.

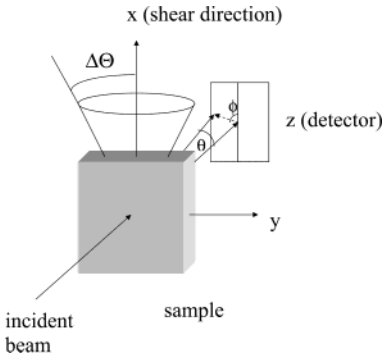

Figure 2. Schematic of experimental setup, showing light scattering and shearing geometry. An anisotropic orientation distribution is represented by a cone making angle $\Delta\Theta$ about the shear flow direction. Grain optic axes are assumed to be confined to this cone. A scattered light ray that is deflected from the forward direction is characterized by the polar angles θ and ϕ.

exhibit 4-fold symmetry. The work in ref 30 was restricted to such systems. However, it is natural that, under some circumstances, the orientation of the optic axes of the misaligned grains may be biased toward the orientation of the optic axis of the single crystal. In such systems, the resulting depolarized light scattering will exhibit 2-fold symmetry. The observation of 2-fold symmetric scattering patterns from sheared or stretched polymer samples dates back to the pioneering work of Stein and co-workers, who attributed this effect to the orientation of anisotropic fibers.[48] In this paper we develop a theoretical model for depolarized light scattering from a biased collection of misaligned uniaxial grains embedded in a macroscopic uniaxial single crystal and apply it to experimental data obtained from a concentrated block copolymer solution under shear flow.

Anisotropic Distribution Model

The grain model that has been the basis for much of our recent work on depolarized light scattering from block copolymer samples assumes that a sample consists of a collection of birefringent (optically anisotropic) grains with constant optic axis within each grain. We calculate an incoherent sum of scattering intensities from individual grains, which is equivalent to averaging over the scattering patterns from a statistical ensemble of sample realizations. The average grain shape is characterized by a Gaussian correlation function in which the characteristic grain size in the direction parallel to the optic axis is different from the characteristic size in the direction perpendicular to the optic axis. Such a correlation function exhibits contour surfaces of constant value that are ellipsoids of revolution.[30] All of our previous studies assume a random distribution of grain orientations. These grains either can fill the whole sample[27] or can coexist with a disordered (isotropic) matrix[12,27] and/or a single-crystalline (anisotropic) matrix.[30]

An earlier study[30] treated the case of a medium with nonzero average background anisotropy, in which the spatially fluctuating part of the dielectric tensor was statistically isotropic, as shown in Figure 1a. The difference between scattering from that medium and from a medium with an isotropic background, was that (1) the angle of the polarizer and analyzer had to be chosen to suppress the birefringence from the anisotropic background and (2) there was an additional small reduction in scattered intensity associated with destructive interference between scattered components generated at different longitudinal locations inside the sample, which was negligible for typical sample parameters. The depolarized scattered beam retained 4-fold symmetry about the axis of propagation of the incident beam.

We now consider scattering from a medium with a background anisotropy and in which the spatially fluctuating part of the dielectric tensor is statistically anisotropic; that is, the distribution of the optic axes of the scatterers is not uniform in solid angle. This situation is depicted in Figure 1b. An incident light wave is assumed to be directed along the z axis, and the polarizer is oriented in the x direction and the analyzer in the y direction. Several features of the experimental configuration allow us to substantially simplify the analysis. First, the optic axis of the background matrix is arranged to be along the x axis (the shear direction), so the polarization of the incident wave remains in the x direction as it propagates through the sample. Second, the sizes of the randomly oriented grains are large enough such that the scattered waves are deflected into a small angular range about the z axis, so that the y component of the scattered field can be considered to remain in the y direction as it propagates through the sample and to the detector. Assuming that the effect of the background anisotropy can again be accounted for in the same way as when the scatterer optic axis orientations were isotropic, the analysis can simply modify that for the case with no background anisotropy by accounting for the nonuniformity of the distribution of scatterer optic axes.

In the present analysis we use the x axis as the polar axis for the distribution of optic axes. For simplicity, the grain orientation distribution is assumed to be uniform over the full range of the azimuthal angles about x, Φ_g. The polar angle measured from x is Θ_g. All previous experiments on shearing cylindrical block copolymers indicate that the cylinder axes are oriented in the flow (x) direction.[49−51] We thus assume that shearing induces the grain optic axes to lie in a cone of angle $\Delta\Theta$ centered around the shearing (x) direction (Figure 2). The limit $\Delta\Theta \rightarrow \pi/2$, describes an isotropic distribution of grain orientations, while the limit $\Delta\Theta \rightarrow 0$ describes perfectly aligned grains, i.e., a perfect single crystal.

The relevant term for depolarized scattering is the $x-y$ matrix element of the deviation of the dielectric tensor from its average value, $(\delta\epsilon/\epsilon_0)_{x,y}$. For those grains whose optic axis make the polar angles $\{\theta_g$ (measured from the z axis), ϕ_g (measured from the x axis in the $x-y$ plane)$\}$ with respect to the direction of the incident

beam (z), we have

$$\left(\frac{\delta\vec{\epsilon}}{\epsilon_0}\right)_{x,y} = \left(\frac{\delta\vec{\epsilon}}{\epsilon_0}\right)_{y,x} = \frac{1}{2}(n_e^2 - n_o^2)\sin^2\theta_g \sin(2\phi_g) = \frac{1}{2}(n_e^2 - n_o^2)\sin(2\Theta_g)\cos\Phi_g \quad (1)$$

where n_e and n_o are the extraordinary and ordinary refractive indices of a grain and ϵ_0 is the permittivity of the vacuum. The general expression for the depolarized scattered light intensity from a collection of uncorrelated ellipsoidal grains with Gaussian shape functions is given by

$$I = \frac{k^4 I_{inc} n^2 (n_e^2 - n_o^2)\phi_{grains} V_s (2\pi)^{3/2} l w^2}{(4\pi)^2} \times \int\int \frac{\sin\theta_g \, d\theta_g \, d\phi_g}{4\pi} \sin^4\theta_g \sin^2(2\phi_g) \exp(-w^2 q^2/2) \times \exp\left(-\frac{(l^2 - w^2)(\mathbf{q}\cdot\mathbf{g})^2}{2}\right) \quad (2)$$

where $\mathbf{q}$ is the scattering vector, $\mathbf{g}$ is a unit vector in the direction of the grain optic axis, l and w are the ellipsoid length parameters in directions parallel and perpendicular to $\mathbf{g}$ respectively, V_s is the illuminated sample volume, ϕ_{grains} is the volume fraction occupied by grains, and I_{inc} is the incident beam intensity. In the paraxial approximation, the Cartesian coordinates of $\mathbf{q}$ are

$$\mathbf{q} = \mathbf{a}_x k \sin\theta\cos\phi + \mathbf{a}_y k \sin\theta\sin\phi = q(\mathbf{a}_x\cos\phi + \mathbf{a}_y\sin\phi) \quad (3)$$

where θ and ϕ are the polar angles of the scattered beam, relative to the polar z axis, and $q = k\sin\theta$. The Cartesian components of the grain axis $\mathbf{g}$ are

$$\mathbf{g} = \mathbf{a}_x\cos\Theta_g + \mathbf{a}_y\sin\Theta_g\cos\Phi_g + \mathbf{a}_z\sin\Theta_g\sin\Phi_g \quad (4)$$

and $\mathbf{q}\cdot\mathbf{g}$ becomes

$$\mathbf{q}\cdot\mathbf{g} = q\cos\phi\cos\Theta_g + q\sin\phi\sin\Theta_g\cos\Phi_g \quad (5)$$

In terms of $\{\Theta_g,\Phi_g\}$, eq 2 becomes

$$I = K\exp(-w^2q^2/2)\int_0^{\Delta\Theta}\frac{\sin\Theta_g\,d\Theta_g}{4\pi}\sin^2(2\Theta_g) \times \exp(-\xi(\theta)(2(\cos\phi\cos\Theta_g)^2 + (\sin\phi\sin\Theta_g)^2))I_{\Phi g} \quad (6)$$

$$I_{\Phi g} = \frac{1}{2}\int_0^{2\pi} d\Phi_g\,(1 + \cos(2\Phi_g))\exp(-\alpha\cos\Phi_g) \times \exp(-\beta\cos(2\Phi_g)) \quad (7)$$

where $\xi(\theta) = (l^2 - w^2)q^2/4$, $\alpha = \xi(\theta)\sin(2\phi)\sin(2\Theta_g)$, and $\beta = \xi(\theta)(\sin\phi\sin\Theta_g)^2$.

Scattering Pattern Symmetry and Series Representation

From eqs 6 and 7, the scattered light intensity has the following symmetries:

$$I(\phi) = I(\phi+\pi) \quad \text{and} \quad I(\phi) = I(-\phi) \quad (8)$$

This ensures a minimum of 2-fold symmetry for all scattering profiles.

Representing the exponentials in the Φ_g integrand by their Fourier series expansions

$$\exp(-\alpha\cos\Phi_g) = \sum_{m=0}^{\infty}\epsilon_m(-1)^m I_m(\alpha)\cos(m\Phi_g)$$

$$\exp(-\beta\cos(2\Phi_g)) = \sum_{m=0}^{\infty}\epsilon_m(-1)^m I_m(\beta)\cos(2m\Phi_g) \quad (9)$$

yields

$$I_{\Phi g} = (\pi/2)\sum_{m=0}^{\infty}\sum_{n=0}^{\infty}\epsilon_m\epsilon_n(-1)^{m+n}I_m(\alpha)\,I_n(\beta) \times \left(\delta(2n-m) + \delta(2n+m) + \frac{1}{2}\delta(2n-m+2) + \frac{1}{2}\delta(2n-m-2) + \frac{1}{2}\delta(2n+m+2) + \frac{1}{2}\delta(2n+m-2)\right) \quad (10)$$

where I_m is the modified Bessel function of order m and $\delta(s) = 1$ if $s = 0$ and zero otherwise. When this form is substituted into eq 6, we get an expression that can be conveniently evaluated numerically. A check on the procedure is provided by the special case $\Delta\Theta = \pi/2$, corresponding to an isotropic distribution, which can be evaluated by a completely different expression. The maximum value of the summation index, n, is chosen so that the expression (eq 10) converges to a numerical integration of eq 7 at the largest value of q (the most severe test of convergence).

Calculations

The anisotropic distribution model just described allows one to calculate scattering patterns as a function of four independent, adjustable parameters: an overall grain size parameter (w), a measure of the aspect ratio (eccentricity) of the ellipsoidal grains (l/w), a scattering intensity scaling factor, which is proportional to the volume fraction of grains (I_0), and the angular range of grain orientations ($\Delta\Theta$). The value of w only affects the overall size of the scattering pattern. Figure 3 shows the calculated 2-D scattering patterns in the q_x–q_y plane, with various l/w and $\Delta\Theta$ values. In all figures representing scattering patterns in this paper, the shear (x) direction is assumed to be in the vertical direction and the q_x and q_y axes are rendered dimensionless by multiplying by the grain size parameter w. In Figure 3a we show the scattering pattern obtained from a sample with randomly oriented ($\Delta\Theta = \pi/2$) grains with a prolate ellipsoidal shape with $l/w = 2.0$. We see an azimuthally asymmetric pattern with 4-fold symmetry and enhanced scattering along the $\phi = \pi/4 + n\pi/2$ directions, where $n = 0$, 1, 2, or 3. The effect of shear on these grains in reciprocal space is shown in Figure 3b, where we show the effect of restricting the orientation angles of the grains to a cone with $\Delta\Theta = \pi/4$ (see Figure 2 for details about the cone). This leads to a compression of the scattering pattern along the q_x direction and stretching of the scattering pattern along the q_y direction. Further restriction of the grain orientation angles leads to further compression along the q_x direction and further stretching along the q_y direction,

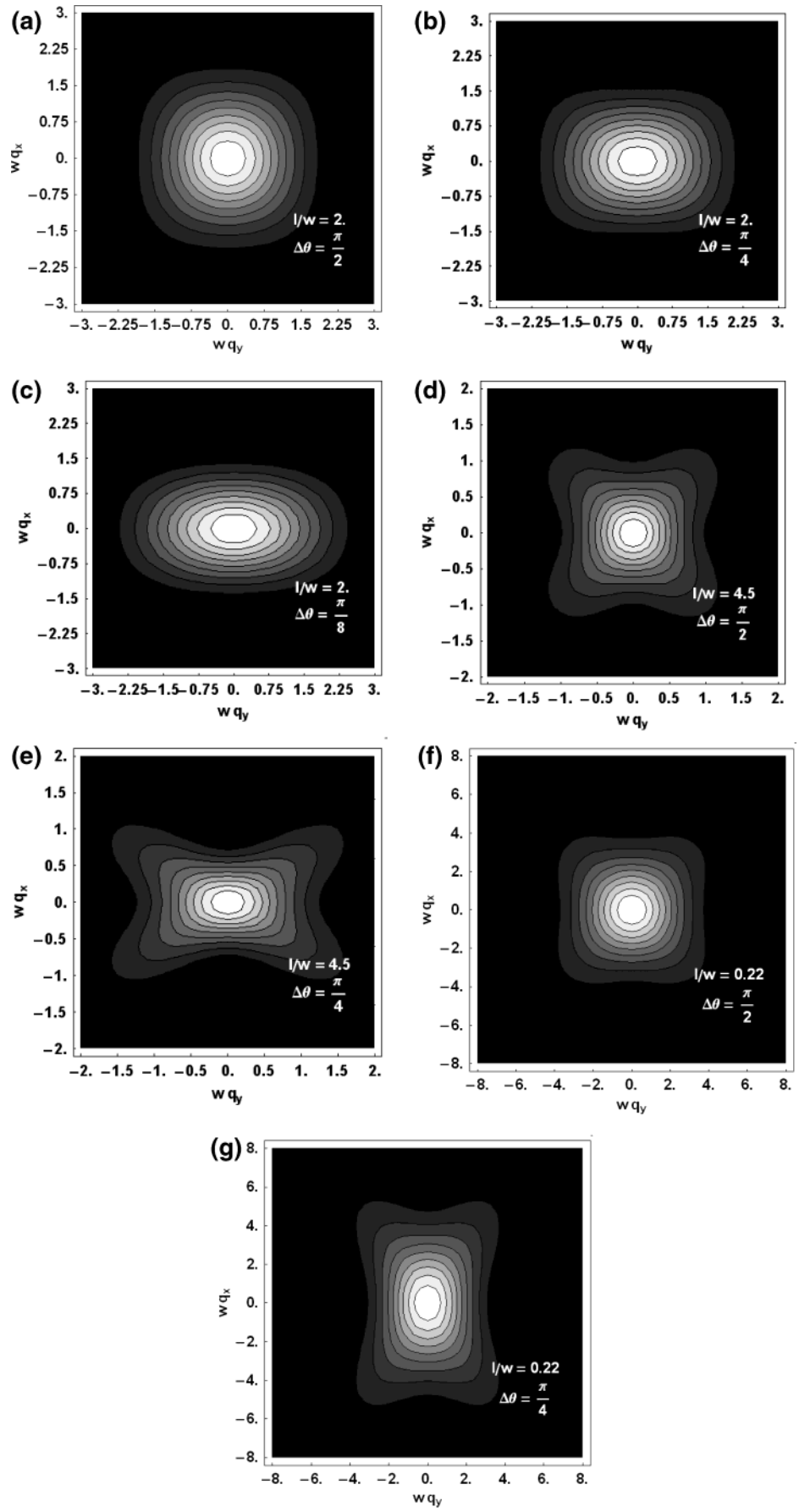

Figure 3. Seven calculated scattering patterns based on the theoretical model. Cases a−g differ in their values of $\Delta\Theta$ and l/w. All x and y axes represent the reduced unitless parameter wq. For all scattering patterns with anisotropic orientation distributions in this paper, the flow direction is assumed to be the vertical (x) direction.

as shown in Figure 3c, where we show results obtained at $\Delta\Theta = \pi/8$.

In Figure 3d we show the scattering pattern obtained from a sample with randomly oriented ($\Delta\Theta = \pi/2$) prolate ellipsoidal grains with $l/w = 4.5$. A comparison of parts a and d of Figure 3 reveals that increasing the eccentricity of the grains leads to an increase in the 4-fold modulation of the scattering patterns. The enhancement of scattering seen along the $\phi = \pi/4$ direction relative to the $\phi = 0$ direction is substantially larger for $l/w = 4.5$ (Figure 3d) than $l/w = 2.0$ (Figure 3a). Restricting the orientation angles of the grains $l/w = 4.5$ to a cone with $\Delta\Theta = \pi/4$ results in compression of the scattering pattern along the q_x direction and stretching along the q_y direction, as shown in Figure 3e.

In Figure 3f we show the scattering pattern obtained from a sample with randomly oriented ($\Delta\Theta = \pi/2$) grains with an oblate ellipsoidal shape with $l/w = 1/4.5 = 0.22$. The ratios of the long to short axes of the grains depicted in Figure 3d,f are thus identical. It is clear that the 4-fold modulation obtained from prolate ellipsoids (Figure 3d) is significantly larger than that obtained from oblate ellipsoids (Figure 3f). However, distinguishing between oblate and prolate ellipsoidal grains is difficult on the basis of depolarized light scattering due to the qualitative similarity of the patterns (Figure 3d,f). In Figure 3g we show the effect of shearing on the oblate grains described in Figure 3f ($l/w = 0.22$) by setting $\Delta\Theta = \pi/4$. As has been the case in all of the previous calculations, we assume that in this case the cylinders lie parallel to the flow direction. The scattering pattern under flow is then predicted to be stretched in the q_x direction and compressed in the q_y direction, as shown in Figure 3g. This result, which is exactly the opposite of what we have seen in the prolate cases ($l/w = 2.0$ and 4.5; Figure 3a−e), is obtained because the oblate grains tend to have their long axes orthogonal to the flow direction.

To a good approximation, the intensity patterns from anisotropic distributions of grains can be expressed as the sum of four terms:

$$I(\theta,\phi) = C_0(\theta) + C_2(\theta)\cos(2\phi) + C_4(\theta)\cos(4\phi) + C_6(\theta)\cos(6\phi) \quad (11)$$

The functions C_0, C_2, C_4, and C_6 can be extracted from theoretically calculated or experimentally measured intensities by calculating cosine transforms of the full intensity data:

$$C_n(\theta) = \int_0^{2\pi} I(\theta,\phi)\cos(n\phi)\,d\phi \quad (12)$$

In our previous treatment of the light scattering patterns from isotropic distributions of grains,[27,30] the scattering patterns have 4-fold symmetry and $I(\theta,\phi)$ is given by a special case of eq 11 with $C_2 = C_6 = 0$:

$$I(\theta,\phi) = C_0(\theta) + C_4(\theta)\cos(4\phi) \quad (13)$$

As was the case with the scattering profiles, it is convenient to use qw as the scaled independent variable instead of θ. We will thus report $C_n(qw)$ in the remainder of this section. Equations 11 and 12 provide a convenient framework for distinguishing between the variety of scattering patterns shown in Figure 3. The integral in eq 12 for $n \leq 6$ was computed numerically for all of the patterns shown in Figure 3a−g, and the resulting $C_n(qw)$'s are shown in Figure 4a−g, respectively. For the quiescent case with $l/w = 2.0$ (Figure 4a), all aspects of the 2-D scattering profile (Figure 3a) from this collection of grains is thus captured by two 1-D profiles, $C_0(qw)$ and $C_4(qw)$ as shown in Figure 4a. $C_0(qw)$ dictates the overall decay of the scattering intensity with increasing q, while $C_4(qw)$ is a measure of the 4-fold modulation. The fact that $C_4(qw) < 0$ for all qw values indicates that the pattern has an "x" shape rather than a "+" shape. The magnitude of C_0 at particular values of qw is larger than that of C_4 by a factor of 10 or more (Figure 4a). This implies a relatively weak 4-fold modulation of the scattering profile. In Figure 4b we show the effect of shear alignment on C_n by setting $\Delta\Theta = \pi/4$. The most important signature of alignment is the development of a nonzero $C_2(qw)$; there is no qualitative change in either the magnitude or sign of $C_0(qw)$ and $C_4(qw)$. The fact that $C_2(qw)$ is negative indicates stretching along the y direction. The magnitude of $C_2(qw)$ is larger than the next higher moment, $C_4(qw)$, indicating that the 2-fold modulation due to alignment overwhelms the mild 4-fold modulation present in the unaligned case. We also see that $C_6(qw)$ is nonzero. However, the magnitude of $C_2(qw)$ is significantly larger than $C_6(qw)$ at all qw. We thus conclude that, for all practical purposes, the features of the anisotropic scattering pattern in Figure 3b are captured by three 1-D functions, $C_0(qw)$, $C_2(qw)$, and $C_4(qw)$. The effect of constraining $\Delta\Theta$ to $\pi/8$ for the $l/w = 2.0$ grains is shown in Figure 4c. As expected, the relative magnitude of $C_2(qw)$ has increased [compare $C_2(qw)$ in Figure 4a,b]. We also see that $C_4(qw)$ is positive; i.e., it has changed sign relative to the $\Delta\Theta = \pi/2$ and $\pi/4$ cases. This change in sign is of little practical importance as the scattering profile features are essentially determined by $C_0(qw)$ and $C_2(qw)$. $C_6(qw)$ remains negligible in all cases (Figure 4a−c).

In Figure 4d we show $C_n(qw)$ of quiescently ordered grains with $l/w = 4.5$. The increase in magnitude of $C_4(qw)$ relative to $l/w = 2.0$ is due to the enhanced 4-fold modulation of the scattering profiles (compare Figure 3a,d). Aligning these grains by setting $\Delta\Theta = \pi/4$ results in a negative $C_2(qw)$ function while the $C_4(qw)$ remains largely unaffected (compare Figure 4d,e). In addition we see that $C_6(qw)$ is no longer negligible. Recall that for the case with $l/w = 2.0$, $C_6(qw)$ was negligibly small for both $\Delta\Theta = \pi/4$ and $\pi/8$. It is obvious that $C_6(qw)$ becomes nonnegligible in aligned cases where the grain eccentricity is large.

In Figure 4f,g we show the effect of alignment on oblate grains with $l/w = 0.22$. The quiescent $C_0(qw)$ and $C_4(qw)$ profiles are similar to those obtained from prolate grains (compare Figure 4d,f). The main difference is in the sheared patterns. Shearing oblate grains with the same eccentricity results in positive $C_2(qw)$ profiles (Figure 4g). In contrast, all prolate sheared cases (Figure 4b,c,e) showed negative $C_2(qw)$ profiles. Here we also find that $C_2(qw)$ is significantly greater than $C_6(qw)$.

In all cases of interest in this work $C_2(qw) \gg C_6(qw)$. For the remainder of the paper we thus assume that

$$I(\theta,\phi) = C_0(\theta) + C_2(\theta)\cos(2\phi) + C_4(\theta)\cos(4\phi) \quad (14)$$

Experimental Section

A polystyrene−polyisoprene diblock copolymer was synthesized by anionic polymerization under high vacuum, using methods described elsewhere.[52] The weight-average molecular

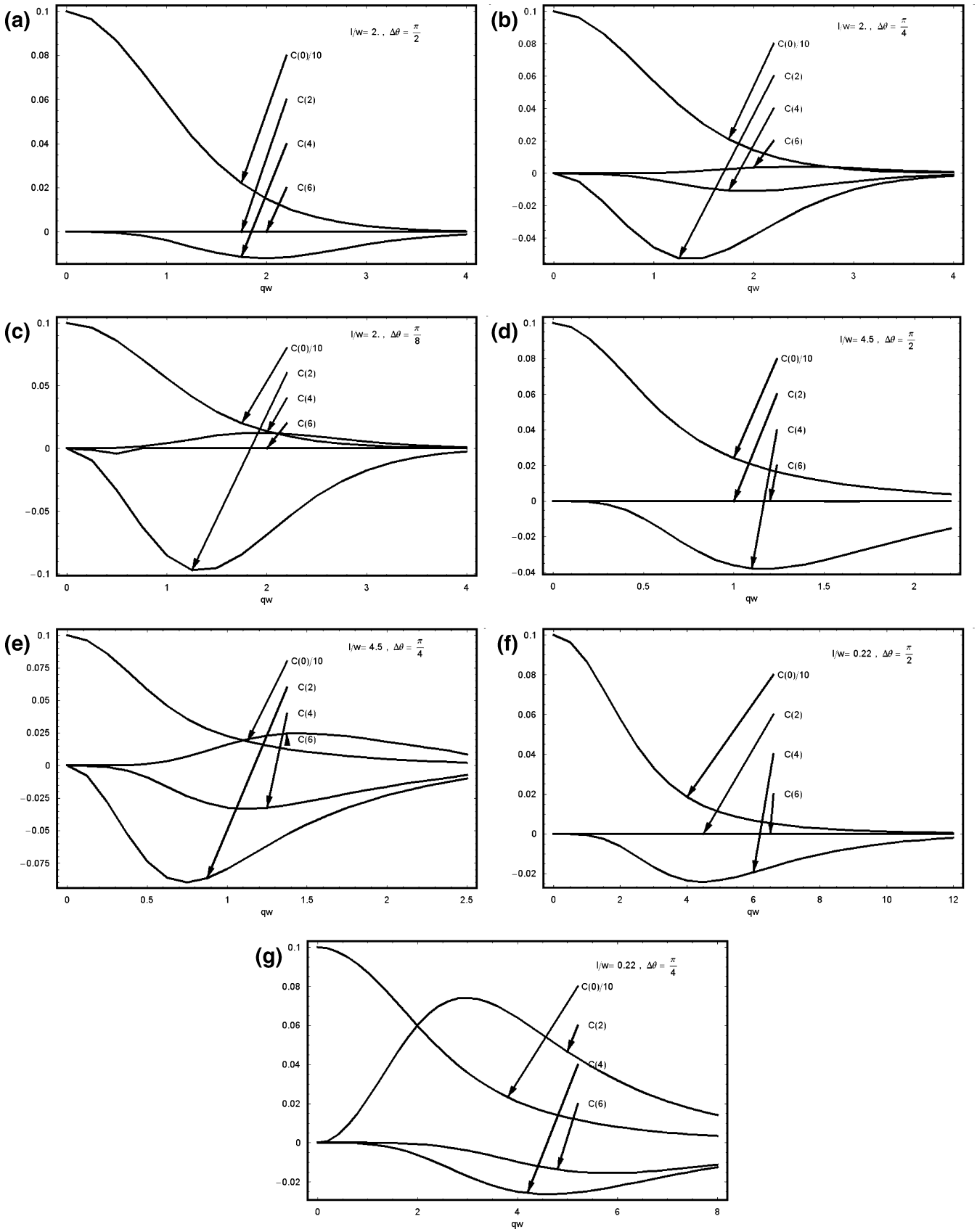

Figure 4. Plots of cosine transforms C_0, C_2, C_4 and C_6 vs wq corresponding to the seven calculated scattering patterns shown in Figure 3.

weights of the polystyrene and polyisoprene blocks were 10 and 30 kg/mol, respectively, and we refer to this polymer as SI(10−30). Based on extensive characterization of polystyrene−polyisoprene block copolymers, we expect the sample to have a cylindrical microstructure. To reduce the order-disorder transition (ODT) temperature to an experimentally accessible range, we prepared a dioctyl phthalate solution (33% DOP) of SI(10−30).

The optical properties of our sample, under quiescent conditions and under reciprocating shear flow, were studied

Table 1. Quiescent DPLS Analysis for 67% SI(10−30) + 33% DOP[a]

time (min)	I_0	l	w	*l*/*w*	v	ϕ_g
0	0	0	0	0	0	0
30	0	0	0	0	0	0
60	6.45	5.1	1.7	3	15	0.37
75	20.1	6.7	1.9	3.5	24	0.70
105	33.4	7.4	2.1	3.5	32	0.85
210	37.8	7.7	2.2	3.5	37	0.85
420	40.1	7.7	2.2	3.5	37	0.90
990	43.4	7.7	2.2	3.5	37	0.98
1065	44.5	7.7	2.2	3.5	37	1

[a] Length parameters (*l*, *w*) are in micrometers, grain volumes (*v*) are in cubic micrometers, and forward scattered intensities (I_0) are in arbitrary units.[57]

using an apparatus described in ref 30. Quiescent birefringence measurements[53−55] indicated that the ODT temperature of our system was 62 ± 2 °C. A 1-mm-thick sample was disordered by heating to 65 °C and then quenched to 45 °C. It took less than 15 min for the sample to reach the final quench temperature after the start of cooling. Time zero is defined as the time when the cooling was started. The quiescent depolarized light scattering pattern from this sample was acquired periodically over about 1000 min, using a HeNe laser (633-nm wavelength) as the light source. A background pattern was also acquired with the laser turned off. This background pattern was subtracted from each scattering pattern. The resultant patterns were all X-shaped with 4-fold symmetry and were analyzed using methods described in ref 30.

Reciprocal shear studies were then performed on our sample, using strain amplitudes of 20, 50, and 200% and shear velocities of 0.1, 0.5, and 1 mm/s. Samples were disordered at 65 °C prior to each shear flow experiment. The sample was then quenched to 45 °C, and the shear flow was started immediately at the beginning of the quench. Both depolarized light scattering (polarizer/analyzer axes set at 0°/90° to shear flow direction) and birefringence (polarizer/analyzer axes set at 45°/135° to shear flow direction) were measured periodically over a time of 200 min. The polarizer and analyzer axes were always orthogonal to each other, and the incident laser beam was always pointed in the velocity gradient direction.

Results and Discussion

The results of quiescent light scattering measurements on the SI(10−30)/DOP solution are shown in Table 1. X-patterns with 4-fold symmetry were observed, with scattered intensity falling off monotonically with increasing *q*, indicating the presence of uncorrelated, ellipsoidal grains. These patterns get smaller and more intense as time progresses, indicating that grains were growing with time and occupying a greater volume fraction of the sample. The sample was mostly (85%) ordered after about 200 min. After 200 min, analysis of light scattering patterns using previously developed methods given in ref 27 indicated prolate ellipsoidal grain sizes leveling off with dimensions $l = 7.7\ \mu$m and $w = 2.2\ \mu$m. Using quiescent light scattering data and birefringence measurements after 1000 min, at which time we could be certain that the sample was completely ordered, we determined that $\Delta n = 1.8 \times 10^{-4}$ for SI(10−30)/DOP; see ref 30 for details regarding data analysis. This value is roughly half that measured for the SI(7−18) melt studied in ref 30. The difference between the two cases is expected due to the presence of a common solvent in the SI(10−30)/DOP discussed here.

Measurements of birefringence, i.e., the fraction of incident light transmitted through crossed polarizers P/P_0, along with knowledge of Δn for a single crystal,

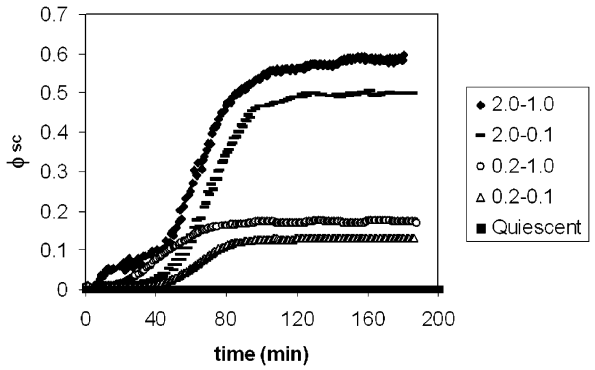

Figure 5. Single-crystal volume fraction vs time for quiescent and sheared SI(10−30)/DOP solutions. The first number in the legend is the fractional shear strain amplitude; the second number is the shear velocity in millimeters per second.

were used to compute the time dependence of the single-crystal volume ϕ_{sc}, obtained under shear flow:[30]

$$\frac{P}{P_0} = \sin^2(\Gamma\phi_{sc}/2) \tag{15}$$

where $\Gamma = 2\pi L\Delta n/\lambda$ and *L* is the sample thickness.

The time dependence of ϕ_{sc} obtained from our sample under different shearing conditions is shown in Figure 5. We find that ϕ_{sc} is a sensitive function of strain amplitude. Increasing it by a factor of 10 increased the single-crystal volume fraction by about 400%. In contrast, increasing shear velocity by a factor of 10 increased the single-crystal volume fraction by only 30% or less.

In our model, the remainder of a completely ordered sample is composed of misaligned grains (volume fraction $\phi_{grains} = 1 - \phi_{sc}$). These misaligned grains can be studied by depolarized light scattering. If these grains are randomly oriented, then the forward scattered intensity, I_0, is proportional to both the average grain volume ($v = lw^2$) and to the volume fraction of grains in the sample. This case was treated in ref 30. If, on the other hand, the misaligned grains are characterized by an anisotropic distribution function, then the relationship between I_0 and grain structure is obtained by setting $q = 0$ in eqs 6 and 7:

$$I_0 = Kv\phi_{grains}F(\Delta\Theta) \tag{16}$$

where

$$F(\Delta\Theta) = \frac{8}{15} - \frac{\cos\Delta\Theta}{2} - \frac{\cos(3\Delta\Theta)}{12} + \frac{\cos(5\Delta\Theta)}{20} \tag{17}$$

and the parameter *K* is given by

$$K = \frac{k^4 I_{inc} n^2 (n_e^2 - n_o^2) V_s (2\pi)^{3/2}}{(8\pi)^2} \tag{18}$$

Equation 16 is identical to that obtained for a randomly oriented collection of misaligned grains[30] except for the $F(\Delta\Theta)$ factor, given in eq 17. Figure 6 shows the dependence of *F* on $\Delta\Theta$. $F(\Delta\Theta)$ reaches its maximum value of 8/15 when $\Delta\Theta = \pi/2$ (isotropic distribution), and it approaches 0 as $\Delta\Theta \rightarrow 0$ (perfect alignment). The isotropic result agrees with our previous calculations.[30] The physical origin of the $\Delta\Theta \rightarrow 0$ result is also clear: if $\Delta\Theta = 0$, then there are no misaligned grains and thus there is no depolarized light scattering signal. What is,

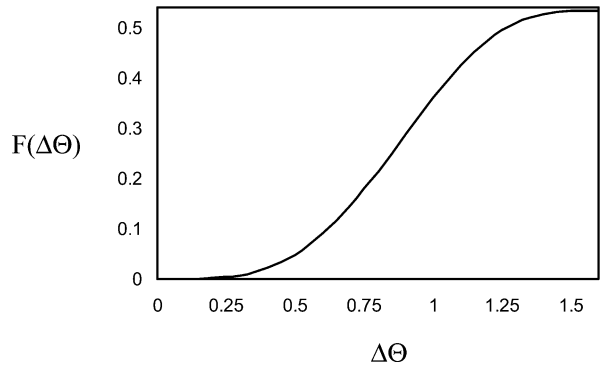

Figure 6. Plot of $F(\Delta\Theta)$ vs $\Delta\Theta$, as described in eq 17, showing how the depolarized scattered intensity changes as the angular width of the orientation distribution changes.

perhaps, surprising are the relatively low values of $F(\Delta\Theta)$ for moderately large values of $\Delta\Theta$. For example, for $\Delta\Theta = \pi/8$, $F = 0.02$ (Figure 6). This implies that the depolarized light scattering intensity from a collection of randomly oriented grains will be 25 times more intense than that obtained from the same collection of grains with optic axes restricted to a cone of 22°. It would thus be extremely difficult to study the properties of misaligned grains with $\Delta\Theta = \pi/8$.

In Figure 7a we show the 2-D depolarized light scattering pattern in the q_x–q_y plane, obtained from our SI(10−30)/DOP solution obtained after shearing the sample for 180 min with a strain amplitude of 0.2 and a strain rate of 1.0 s^{-1}. For $|q| \leq 0.081\ \mu m^{-1}$, leakage of the incident laser beam through the crossed polarizers dominates the pattern, so these small-$|q|$ data are not used in the analysis. This leakage, which typically amounts to about 1% of the scattered light, does not contribute significantly to the analysis of either the depolarized light scattering signal or the birefringence signal.[25] Visual inspection of Figure 7a indicates the presence of a speckle pattern—a random high-spatial frequency intensity modulation that results from the optical interference of light scattering from widely separated grains having parallel optic axes for the particular arrangement of grains found in a given sample. This speckle represents noise in our data, and also makes it difficult to compare experimental results with theoretical curves, which are based on the average scattered intensity from a statistical ensemble of sample realizations, which exhibits no speckle. In previous experiments involving 4-fold symmetric scattering patterns, we could average the scattering data over four equivalent directions to reduce the speckle, but that is not possible in the present case due to the lower symmetry. The speckle patterns were therefore minimized by convoluting the raw data $[I(q_x,q_y)]$ with a two-dimensional Gaussian function whose full width at half-maximum (fwhm) was 20 pixels. Mathematically this is equivalent to filtering the two-dimensional Fourier transform of the raw data, and then taking the inverse transform. The result of this operation on the data in Figure 7a is shown in Figure 7b. It is clear that the filtering process effectively removes the speckle that was in the raw data, allowing more precise fits to theoretical parameters. The scattering profile under shear (Figure 7) are clearly stretched in the y direction and compressed in the x direction. This is most clearly seen in Figure 7b.

In Figure 8a we show the 2-D depolarized light scattering data obtained from our sample under quiescent conditions at $t = 990$ min when the disorder-to-order transition is complete (see Table 1). Figure 8b shows the filtered 2-D scattering data using the same method as that used on the data obtained under shear flow (Figure 7a).

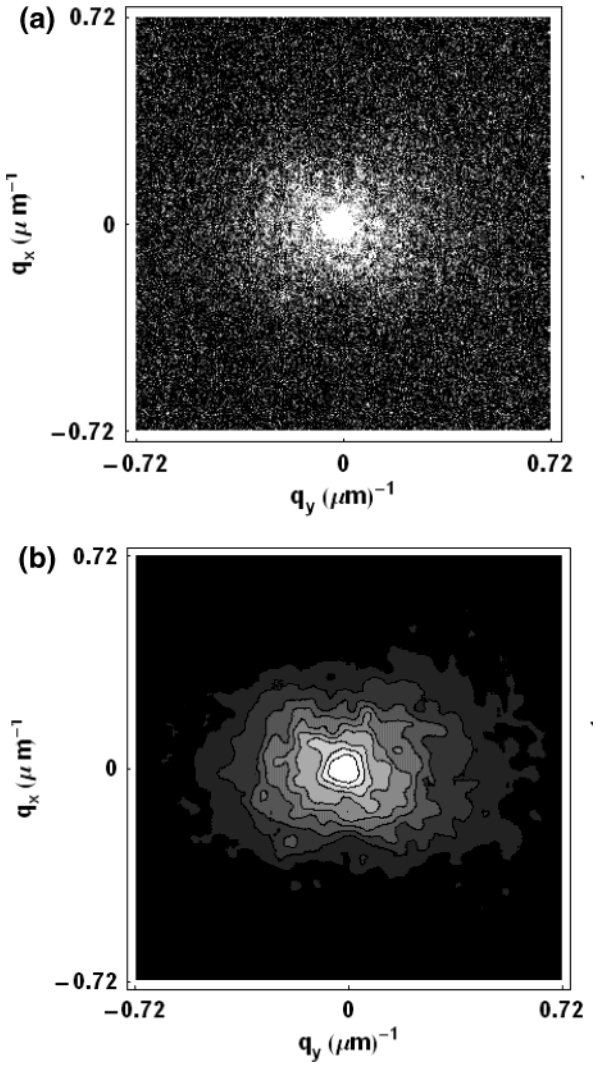

Figure 7. Experimental scattering pattern from a sheared SI(10−30)/DOP solution (20% strain, 1 mm/s, 1 mm thick, $t =$ 180 min): (a) raw intensity data; (b) contour plot after spatial filtering.

Equation 12 was applied to the filtered data in Figures 7b and 8b to extract cosine transform functions $C_0(q)$, $C_2(q)$, and $C_4(q)$. These functions are shown in Figure 9 for the scattering data obtained under shear, shown in Figure 7. A constant background component of C_0 has been subtracted so that C_0 goes asymptotically to zero at large q. The functions C_2 and C_4 are both negative for all q. This is consistent with the theoretical curve shown in Figure 4b. Also shown in Figure 9 are theoretically calculated $C_0(q)$, $C_2(q)$, and $C_4(q)$ functions. A trial-and-error method was used to obtain the best match between theory and experiment.[56] The theoretical curves in Figure 9 correspond to $\Delta\Theta = \pi/4$, $l/w = 2.25$, $I_0 = 105$ (in arbitrary units), and $w = 3.1\ \mu$m.[57] The theoretical and experimental C_n curves in Figure 9 are in remarkable agreement. The function C_0 is maximum at $q = 0$ and decreases monotonically with increasing q, in both theory and experiment. The experimentally determined $C_2(q)$ is negative at all q values with a pronounced minimum at $q = 0.20\ \mu m^{-1}$. This is in near

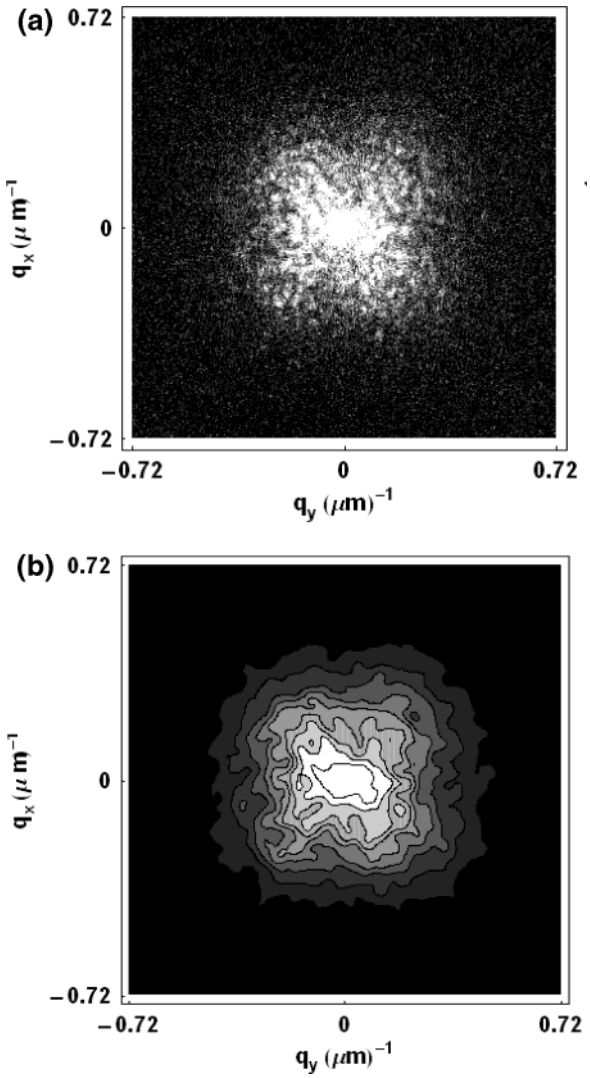

Figure 8. Experimental scattering pattern from quiescently ordered SI(10−30)/DOP solution (1 mm thick, t = 990 min): (a) raw intensity data: (b) contour plot after spatial filtering.

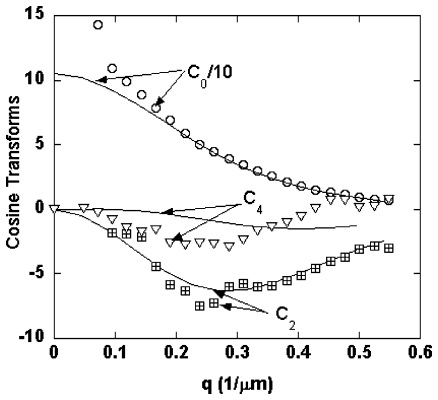

Figure 9. Plots of cosine transforms C_0, C_2, and C_4 vs q calculated from the filtered intensity data shown in Figure 7b (symbols), along with best fit to the four-parameter model (solid line).

quantitative agreement with the theoretical predictions which give a minimum at $q = 0.17\ \mu m^{-1}$. The experimental and theoretical $C_4(q)$ curves have minima at finite q. The experimentally determined $C_4(q)$ has a minimum at $q = 0.17\ \mu m^{-1}$, while the theoretical curve has a minimum at a considerably larger value of q (0.28 μm^{-1}). Perhaps this is due to the fact that the magnitude of $C_4(q)$ is considerably smaller than that of $C_2(q)$. It is thus more difficult to extract this function from the experimental data with high accuracy.

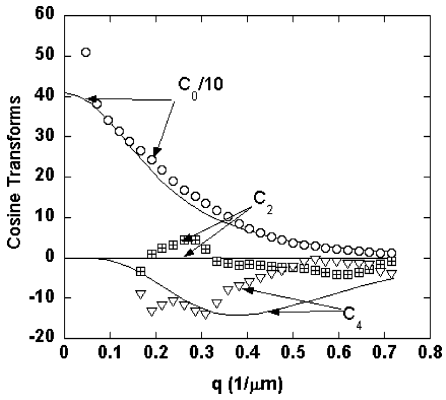

Figure 10. Plots of cosine transforms C_0, C_2, and C_4 vs q calculated from the filtered intensity data shown in Figure 8b (symbols), along with best fit to the four-parameter model (solid line).

The cosine transform functions, obtained from an analysis of the filtered quiescent data (Figure 8b), are shown in Figure 10. Also shown in Figure 10 are the theoretical curves obtained from our trial-and-error procedure which yields $\Delta\Theta = \pi/2$, $l/w = 4$, $I_0 = 400$, and $w = 2.3\ \mu m$. It is gratifying that the best fit was obtained with $\Delta\Theta = \pi/2$, i.e., a random orientation distribution. The theory captures the experimentally determined q dependence of C_0 quantitatively. As expected, the experimentally determined $C_2(q)$ fluctuates around zero while the theoretical $C_2(q)$ is identically zero at all q. The experimentally determined $C_4(q)$ is substantially larger than $C_2(q)$ and negative at all q values, in accordance with theory. Both theory and experiment indicate the presence of a shallow minimum in $C_4(q)$, although this minimum is centered at $q \approx 0.25\ \mu m^{-1}$ for the experimental pattern and at $q \approx 0.35\ \mu m^{-1}$ for the theoretical pattern. It is clear that the proposed model captures the essential features of depolarized light scattering samples with both isotropic and anisotropic grain orientation distributions.

In our previously published analysis of obtaining grain parameters,[27,30] the theoretical and experimental matching of the depolarized light scattering profiles was restricted to $\phi = 0$ and $\pi/4$ directions. This method when applied to the scattering data in Figure 8b gives $l/w = 3.5$ and $w = 2.2\ \mu m$. The values obtained from the present analysis ($l/w = 4.0$ and $w = 2.3\ \mu m$) are probably more reliable because data obtained at all ϕ values have been used.

All our fits described in Figures 9 and 10 indicate the presence of prolate ellipsoids with $l/w > 1$. Attempts to fit the experimental data in Figure 9 using values of $l/w < 1$ led to worse fits than the ones presented in Figure 9. We thus conclude that our sample contains grains with a prolate ellipsoidal shape. In addition, the presence of oblate grains with cylinders aligned in the flow direction would have led to scattering patterns stretched along the x direction (Figure 3g). In contrast, the experimental scattering patterns obtained under flow are stretched in the y direction (Figure 7). This result is also indicative of grains with a prolate ellipsoidal shape.

There has been some debate in the literature regarding the shape of block copolymer grains with cylindrical microstructure.[13,14,27] At infinitesimal quench depths,

where the interfacial tension between the ordered and disordered phases is the dominant driving force that determines grain shape, one expects to obtain oblate grains; see arguments given in refs 13, 14, and 27. At finite quench depths, however, one could obtain prolate grains, if the grain growth rate along the cylinder axis is faster than that perpendicular to it. Both kinds of grains have been reported in the literature. While the quiescent scattering patterns from both prolate and oblate ellipsoids are qualitatively similar (Figure 4d,f), their response to shear flow is qualitatively different (Figure 4e,g). We therefore conclude that under our experimental conditions involving relatively deep quenches (17 °C below the order−disorder transition temperature) prolate grains are obtained due to the kinetic control of grain shape.

Using the quiescent results at long times ($\Delta\Theta = \pi/2$, $l/w = 4.0$, $I_0 = 400$, $w = 2.3\ \mu$m, $F = 8/15$, and $\phi_{grains} = 1$), the parameter K in eq 16 is 15.4. This enables calculation of the volume fraction of misaligned grains at a strain amplitude of 0.2 and a strain rate of 1.0 s^{-1} (data in Figure 7), because all of the other parameters in eq 16 have been measured: $\Delta\Theta = \pi/4$, $l/w = 2.25$, $I_0 = 105$, $w = 3.1\ \mu$m, and $F = 0.20$. Using these parameters, we determined that $\phi_{grains} = 0.5 \pm 0.3$, based on the estimated uncertainties in w of $\pm 0.5\ \mu$m. The volume fraction of the single crystal obtained from the birefringence measurements, $\phi_{sc} = 0.2$ (Figure 5), so that the sum $\phi_{grains} + \phi_{sc}$ is about 0.7 ± 0.3. This is consistent with the expectation that at long times $\phi_g + \phi_{sc}$ should be close to unity; i.e., the sample is completely ordered. For the experiments with strain amplitude of 2.0 and strain rate of 1.0 s^{-1}, the data in Figure 5 indicate that $\phi_{sc} = 0.6$. However, we were unable to detect any depolarized light scattering intensity signal under these conditions, suggesting that either $F \approx 0$ or $\phi_{grains} \approx 0$, so we cannot estimate the magnitude of $\phi_{grains} + \phi_{sc}$, except to say that it is ≥ 0.6. It is possible that there is a substantial volume fraction of grains in this case but that their orientations are so close to the shear direction that they do not produce any measurable light scattering signals.

Concluding Remarks

The grain structure of partially aligned block copolymers with cylindrical morphology was studied by in-situ measurements of optical birefringence and depolarized light scattering under shear flow. Our samples exhibited depolarized scattering patterns with 2-fold symmetry. They were compressed in the flow direction and stretched in the vorticity direction. We demonstrated that these patterns arise due to the presence of an anisotropic distribution of unaligned ellipsoidal grains imbedded in a single crystal. We developed a model for obtaining the properties of the aligned single crystal and those of the unaligned grains. The model enabled computation of theoretical scattering patterns given four parameters: grain size, grain aspect ratio, grain volume fraction, and angular range of orientation distribution. Scattering intensities of patterns with 2-fold symmetry tend to be weak due to weak depolarized scattering from grains whose optic axes are nearly parallel to the shear flow direction. A new method for analyzing these patterns was developed on the basis of cosine transforms of the 2-D experimental scattering patterns. The essential features of the 2-D data were captured by three 1-D functions $C_0(q)$, $C_2(q)$, and $C_4(q)$. By comparing the experimentally determined $C_n(q)$ functions with theoretical calculations, we obtained the structure of the sample under shear flow (at strain amplitude of 0.2 and a strain rate of 1.0 s^{-1}). We determined that the optic axes of the misaligned grains that coexisted with the single crystal under flow were restricted to an angle of 45° to the shear flow direction. The size and eccentricity of the grains under flow were within a factor of 2 of values obtained under quiescent conditions. The framework that we have developed can be applied to any sample composed of a partially aligned collection of weakly birefringent grains and thus might be used to characterize other systems such as processed crystalline and liquid crystalline polymers.

Acknowledgment. Financial support provided by the National Science Foundation (Grant No. DMR-0213508) is gratefully acknowledged.

References and Notes

(1) Bates, F. S.; Fredrickson, G. H. *Annu. Rev. Phys. Chem.* **1990**, *41*, 525.
(2) de Gennes, P. G.; Prost, J. *The Physics of Liquid Crystals*, 2nd ed.; Clarendon Press: Oxford, England, 1993.
(3) Leibler, L. *Macromolecules* **1980**, *13*, 1602.
(4) Fredrickson, G. H.; Helfand, E. *J. Chem. Phys.* **1987**, *87*, 697.
(5) Matsen, M. W.; Bates, F. S. *Macromolecules* **1996**, *29*, 1091.
(6) Hamley, W. *Physics of Block Copolymers*; Oxford University Press: Oxford, England, 1996.
(7) Brazovskii, S. A. *Sov. Phys. JETP* **1975**, *41*, 85.
(8) Gido, S. P.; Gunther, J.; Thomas, E. L.; Hoffman, D. *Macromolecules* **1993**, *26*, 4506.
(9) Park, M.; Harrison, C.; Chaikin, P. M.; Register, P. A.; Adamson, D. H. *Science* **1997**, *276*, 1401, and references therein.
(10) Thurn-Albrecht, T.; Schotter, J.; Kastle, G. A.; Emley, N.; Shibauchi, T.; Krusin-Elbaum, L.; Guarini, K.; Black, C. T.; Touminen, M. T.; Russell, T. P. *Science* **2000**, *290*, 2126, and references therein.
(11) Garetz, B. A.; Balsara, N. P.; Dai, H. J.; Wang, Z.; Newstein, M. C.; Majumdar, B. *Macromolecules* **1996**, *29*, 4675.
(12) Chang, M. Y.; Abuzaina, F. M.; Kim, W. G.; Garetz, B. A.; Newstein, M. C.; Balsara, N. P.; Yang, L.; Gido, S. P.; Cohen, R. E.; Boontonkong, Y.; Bellare, A. *Macromolecules* **2002**, *35*, 4437.
(13) Sakamoto, N.; Hashimoto, T. *Macromolecules* **1998**, *31*, 8493.
(14) Hashimoto, T.; Sakamoto, N. *Macromolecules* **1995**, *28*, 4779.
(15) Segalman, R. A.; Yokoyama, H.; Kramer, E. J. *Adv. Mater.* **2001**, *13*, 1152, and references therein.
(16) Hahm, J.; Lopes, W. A.; Jaeger, H. M.; Sibener, S. J. *J. Chem. Phys.* **1998**, *109*, 10111.
(17) Harrison, C.; Adamson, D. H.; Cheng, Z.; Sebastian, J. M.; Sethuraman, S.; Huse, D. A.; Register, R. A.; Chaikin, P. M. *Science* **2000**, *290*, 1558.
(18) Harrison, C.; Cheng, Z.; Sethuran, S.; Huse, D.; Chaiken, P. M.; Vega, D. A.; Sebastian, J. M.; Register, R. A.; Adamson, D. H. *Phys. Rev. E* **2002**, *66*, 011706.
(19) Sivaniah, E.; Genzer, J.; Fredrickson, G. H.; Kramer, E. J.; Xiang, M.; Li, X.; Ober, C. K.; Magonov, S. *Langmuir* **2001**, *17*, 4342.
(20) Heier, J.; Sivaniah, E.; Kramer, E. J. *Macromolecules* **1999**, *32*, 9007.
(21) Kumaki, J.; Hashimoto, T. *J. Am. Chem. Soc.* **2003**, *125*, 4907.
(22) Laurer, J. H.; Fung, J. C.; Sedat, J. W.; Smith, S. D.; Samseth, J.; Mortensen, K.; Agard, D. A.; Spontak, R. J. *Langmuir* **1997**, *13*, 2177.
(23) Jinnai, H.; Kajihara, T.; Watashiba, Y.; Spontak, R. *Phys. Rev. E* **2001**, *64*, 010803 (R).
(24) Laurer, J. H.; Hajduk, D. A.; Fung, J. C.; Sedat, J. W.; Smith, S. D.; Gruner, S. M.; Agard, D. A.; Spontak, R. J. *Macromolecules* **1997**, *30*, 3938.
(25) Garetz, B. A.; Newstein, M. C.; Dai, H. J.; Jonnalagadda, S. V.; Balsara, N. P. *Macromolecules* **1993**, *26*, 3151.
(26) Newstein, M. C.; Garetz, B. A.; Dai, H. J.; Balsara, N. P. *Macromolecules* **1995**, *28*, 4587.
(27) Newstein, M. C.; Garetz, B. A.; Balsara, N. P.; Chang, M. Y.; Dai, H. J. *Macromolecules* **1998**, *31*, 64.

(28) Milner, S. T.; Morse, D. C. *Phys. Rev. E* **1996**, *54*, 3793.
(29) Balsara, N. P.; Marques, C. M.; Garetz, B. A.; Newstein, M. C.; Gido, S. P. *Phys. Rev. E* **2002**, *66*, 052802.
(30) Wang, H.; Newstein, M. C.; Chang, M. Y.; Balsara, N. P.; Garetz, B. A. *Macromolecules* **2000**, *33*, 3719.
(31) Pinheiro, B. S.; Hajduk, D. A.; Gruner, S. M.; Winey, K. I. *Macromolecules* **1996**, *29*, 1482.
(32) Gupta, V. K.; Krishnamoorti, R.; Kornfield, J. A.; Smith, S. D. *Macromolecules* **1995**, *28*, 4464.
(33) Patel, S. S.; Larson, R. G.; Winey, K. I.; Watanabe, H. *Macromolecules* **1995**, *28*, 4313.
(34) Winey, K. I.; Patel, S. S.; Larson, R. G.; Watanabe, H. *Macromolecules* **1993**, *26*, 2542.
(35) Chen, Z.-R.; Issaian, A. M.; Kornfield, J. A.; Smith, S. D.; Grothaus, J. T.; Satkowski, M. M. *Macromolecules* **1997**, *30*, 7096.
(36) Winey, K. I.; Patel, S. S.; Larson, R. G.; Watanabe, H. *Macromolecules* **1993**, *26*, 4373.
(37) Wang, H.; Newstein, M. C.; Krishnan, A.; Balsara, N. P.; Garetz, B. A.; Hammouda, B.; Krishnamoorti, R. *Macromolecules* **1999**, *32*, 3695.
(38) Gupta, V. K.; Krishnamoorti, R.; Chen, Z.-R.; Kornfield, J. A.; Smith, S. D.; Satkowski, M. M.; Grothaus, J. T. *Macromolecules* **1996**, *29*, 875.
(39) Tsori, Y.; Andelman, D. *Macromolecules* **2002**, *35*, 5161.
(40) Luo, K.; Yang, Y. *Macromolecules* **2002**, *35*, 3722.
(41) Mortensen, K.; Theunissen, E.; Kleppinger, R.; Almdal, K.; Reynaers, H. *Macromolecules* **2002**, *35*, 7773.
(42) Thurn-Albrecht, T.; DeRouchey, J.; Russell, T. P.; Kolb, R. *Macromolecules* **2002**, *35*, 8106.
(43) Koppi, K. A.; Tirrell, M.; Bates, F. S. *Phys. Rev. Lett.* **1993**, *70*, 1449.
(44) Goulian, M.; Milner, S. T. *Phys. Rev. Lett.* **1995**, *74*, 1775.
(45) Cates, M. E.; Milner, S. T. *Phys. Rev. Lett.* **1989**, *62*, 1856.
(46) Balsara, N. P.; Hammouda, B. *Phys. Rev. Lett.* **1993**, *72*, 360.
(47) Zhang, Y.; Wiesner, U. *J. Chem. Phys.* **1995**, *103*, 4784.
(48) Stein, R. S. In *Electromagnetic Scattering; Proceedings*, Kerker, M., Ed.; Macmillan: New York, 1963; p 439.
(49) Folkes, M. J.; Keller, A. *Polymer* **1971**, *12*, 222.
(50) Almdal, K.; Bates, F. S.; Mortensen, K. *J. Chem. Phys.* **1992**, *96*, 9122.
(51) Balsara, N. P.; Dai, H. J.; Kesani, P. K.; Garetz, B. A.; Hammouda, B. *Macromolecules* **1994**, *27*, 7406.
(52) Lin, C. C.; Jonnalagadda, S. V.; Kesani, P. K.; Dai, H. J.; Balsara, N. P. *Macromolecules* **1994**, *27*, 7769.
(53) Amundson, K. R.; Helfand, E.; Patel, S. S.; Quan, X.; Smith, S. S. *Macromolecules* **1992**, *25*, 1953.
(54) Balsara, N. P.; Perahia, D.; Safinya, C. R.; Tirrell, M.; Lodge, T. P. *Macromolecules* **1992**, *25*, 3896.
(55) Balsara, N. P.; Garetz, B. A.; Dai, H. J. *Macromolecules* **1992**, *25*, 6072.
(56) The first step involves generating a set of theoretical scattering patterns covering a range of l/w and $\Delta\Theta$ and finding the pattern that best matches the shape of the experimental scattering pattern, thus determining the best values of l/w and $\Delta\Theta$. One then scales the theoretical C_n curves to match the experimental curves by varying w to match the horizontal scaling and I_0 to match the vertical scaling. In addition, during the matching process one looks at other values of l/w and $\Delta\Theta$ near the first choice. In the future we plan to develop a procedure for the least-squares fitting of these functions in order to extract values of the four parameters w, l/w, I_0, and $\Delta\Theta$ from experimental scattering data.
(57) The l and w values listed throughout this paper are the same as those in refs 12, 25, 27, and 30 but smaller by a factor of $\sqrt{2}$ than those in ref 11. These differences arise because of differences in the forms of the correlation functions used. The I_0 values given in Table 1 are a factor of 2π smaller than those discussed in the text because the newer analysis method is based on integrating image data over the full range of azimuthal angles ($0-2\pi$).

MA035808T